Polyhedron 189 (2020) 114705

Contents lists available at ScienceDirect

Polyhedron

journal homepage: www.elsevier.com/locate/poly

Radical cation salts of *BETS* and *ET* with dicyanamidocuprate anions demonstrating metal-insulator and semiconductor–semiconductor transitions

Nataliya D. Kushch [a], Vyacheslav A. Kopotkov [a,*], Gennady V. Shilov [a], Alexander V. Akimov [a], Sergey V. Tokarev [a], Eduard B. Yagubskii [a,*], Vladimir N. Zverev [b,c], Salavat S. Khasanov [b], Stephen M. Winter [d], Harald O. Jeschke [e]

[a] *Institute of Problems of Chemical Physics RAS, Chernogolovka 142432, MD, Russia*
[b] *Institute of Solid State Physics, RAS, Chernogolovka 142432, MD, Russia*
[c] *Moscow Institute of Physics and Technology, Dolgoprudnyi 141700, MD, Russia*
[d] *Institute for Theoretical Physics, Goethe-Universität, Frankfurt am Main 60438, Germany*
[e] *Research Institute for Interdisciplinary Science, Okayama University, Okayama 700-8530, Japan*

ARTICLE INFO

Article history:
Received 25 May 2020
Accepted 20 July 2020
Available online 24 July 2020

Keywords:
Radical cation salt
Dicyanamidocuprate
Conductivity
Crystal and electronic structure
Pressure effect
Phase transition

ABSTRACT

Electrocrystallization of bis(ethylenedithio)tetraselenafulvalene (BETS) and bis(ethylenedithio)tetrathiafulvalene (ET) in the presence of an electrolyte $(Ph_4P)[Cu(dca)]_3{\cdot}H_2O$ [(dca) = $N(CN)_2$] has been studied using different solvents. A new organic metal $(BETS)_2Cu(dca)_3$ (**1**), and the first radical cation salt with 3D dicyanamidocuprate anion, incorporating both diamagnetic Cu^{1+} and paramagnetic Cu^{2+}atoms, $(ET)_2Cu_{1.8}(dca)_4$ (**2**) have been obtained. Crystal structure, conducting properties of both salts, as well as the electronic structure of **2** and its structural analog $(ET)_2CuMn(dca)_4$ (**3**) were analysed. The salts **1** and **2** have layered structures. In contrast to the BETS radical cation salt **1**, complex **2** is characterized by the presence of a 3D polymeric anion built into the ET radical cation layers. At ambient pressure, the resistance of the crystals **1** shows semimetal behaviour down to 30 K. Below 30 K, the resistance sharply increases and the sample becomes insulating. The application of a pressure of about 3 kbar suppresses the metal-insulator transition. The salt **2** undergoes a semiconductor I - semiconductor II phase transition, which is manifested by a jump in the resistance and a hysteresis in the *R(T)* curves in a very large temperature range (185 – 250 K). The phase transition is accompanied by changes in the charge state of the ET molecules, and notable structure changes in the anion layer, especially in the environment of Cu^{2+}. For the salt **3** the calculated selfconsistent charges show upon cooling a sharp increase of charge order between 291 K and 285 K.

1. Introduction

Radical cation salts on the basis of organic chalcogen-containing π-donors and paramagnetic metal-complex anions combine in one crystallographic lattice conductive and magnetic properties. Conductivity is provided by mobile electrons in organic layers whereas magnetism usually is associated with localized spins of transition metal ions from insulating counter-ion layers. To date, there are known examples of organic metals and superconductors with localized magnetic moments [1–3], molecular antiferromagnetic metals and superconductors [4,5], as well as molecular ferromagnetic metals [6]. The combination of these properties in crystals as well as their synergism, sometimes result in unique molecular materials and magnetic properties [7–11]. In some radical cation salts, for example in λ-$(BETS)_2FeCl_4$ [8,9], κ-$(BETS)_2FeBr_4$ [9], κ-$(BDA\text{-}TTP)_2FeCl_4$ [10], κ-$(BETS)_2Mn(dca)_3$ [11,12], it was found that there are π-*d* interactions between the conducting and magnetic subsystems, which makes it possible to control their conductivity by an external magnetic field [9]. In particular, in λ-$(BETS)_2FeCl_4$ and κ-$(BETS)_2FeBr_4$ salts, field-induced superconductivity was observed [5,8]. Very recently, the first radical cation salts with single-molecule magnets (SMMs) as counter-ions were synthesized [13,14]. An interesting example is the highly conducting single molecule magnet $(BEDO)_4[ReF_6]{\cdot}6H_2O$, whose conductivity

* Corresponding authors.
E-mail addresses: slavaoven@mail.ru (V.A. Kopotkov), yagubski@gmail.com (E.B. Yagubskii).

https://doi.org/10.1016/j.poly.2020.114705
0277-5387/

and monomolecular magnetism coexist in the same temperature range [15]. A combination of two externally controllable physical properties within the radical cation salts allows for the development of molecular spintronic devices [16]. It is known that both simple dicyanamides (dca^-) of *d*-metals and their anionic complexes are characterized by a huge structural diversity [17] and possess different magnetic properties [18,19]. This, in turn, allows for the realization in bifunctional radical cation salts with dicyanamidometalate anions of various types of magnetic orderings and, possibly, synergism along with various conductive properties. To date, there are four radical cation salts of ET and BETS (see Scheme 1) with dicyanamidometalate anions: $(ET)_2Mn(dca)_3$ [19], $(ET)_2CuMn(dca)_4$ (**3**) [20], κ-$(BETS)_2Mn(dca)_3$ (**4**) [11] and κ-$(BETS)_2Co_{0.13}Mn_{0.87}(dca)_3$ (**5**) [21].

For the ET salt **3** with diamagnetic Cu^{+1} and paramagnetic Mn^{2+} ions in its composition, two first order phase transitions were observed as a function of temperature. In the temperature range 291 – 295 K, a hysteretic semiconductor I-semiconductor II transition was observed *via* resistivity and X-ray structural analysis [20]. This transition was attributed to the redistribution of charges between the ET radical cations in the conducting layer. Hysteretic changes in the anisotropic EPR shifts were further detected in the range of 120 – 180 K, evidencing a second transition as result of the distortions in the two-dimensional anion plane formed by the ions of bivalent Mn [22]. The origin and nature of these transitions have not yet been fully revealed.

Crystals of the κ-phase salt **4** show a metal-insulator (M-I) transition at 22 K [23–25]. In the dielectric state, a long-range order of the antiferromagnetic type is observed in the BETS sublattice, as a result of π- electron spin localization. In the anion sublattice below the M-I transition temperature, the *d*-electron Mn^{2+} spins show a tendency towards antiferromagnetic ordering without the formation of a static long-range order due to frustration in the triangular arrangement of Mn^{2+} ions. Interestingly, the transition is completely suppressed by the pressure $P \cong 0.6$ kbar and the salt becomes a superconductor with $T_c = 5.8$ K.

Herein, we present the original successful procedures of the synthesis of new radical cation salts κ-$(BETS)_2Cu(dca)_3$ (**1**) and $(ET)_2Cu_{1.8}(dca)_4$ (**2**) with dicyanamidocuprate anions, as well as crystal and band structures, conducting and magnetic properties. These new salts **1** and **2** are isostructural with previous Mn-based salts **4** and **3**, respectively, thus offering a novel point of comparison for the varied electronic and magnetic properties of the previously reported salts.

2. Experimental section

2.1. Materials and methods

All solvents were obtained chemically clean or extremely clean from Sigma-Aldrich and have been used without further purification. Donors BETS and ET have been recrystallized from CB (chlorobenzene).

2.2. Synthesis of the electrolyte $(Ph_4P)Cu(dca)_3{\cdot}H_2O$

Crystals of the electrolyte were prepared according to the procedure described in [26]. Anal. calc. for $C_{30}H_{22}N_9OPCu$ (619,08): C, 58.20; H, 3.58; N, 20.37; Cu, 10.57%. Found: C, 57.80; H, 3.56; N, 19.69; Cu, 10.20%.

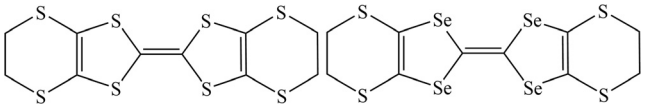

Scheme 1. Donor molecules BETS and ET (or BEDT-TTF). ET (left), BETS (right).

2.3. Synthesis of the salt $BETS_2Cu(dca)_3$ (**1**)

The crystals **1** were obtained by electrochemical oxidation of BETS (C1 = 0.0065 g, 0.011 mmol) in presence of the supporting electrolyte $(Ph_4P)Cu(dca)_3{\cdot}H_2O$, (*C*2 = 0.040 mg, 0.067 mmol) in a mixture of chlorobenzene (CB, 20 mL) – dichloromethane (DCM, 5 mL). The reaction was performed at constant current, I = 0.5 μA, at 25 K in Ar atmosphere. The synthesis was carried out in a glass H-like two-electrode cell with cathodic and anodic chambers separated by a porous glass membrane. The electrodes were 1 mm-diameter platinum wire, electrochemically purified in a 0.1 N sulfuric acid solution. The hexagon-like crystals **1** formed on the anode in two weeks. A preliminary analysis of the crystal composition determined by ERMA showed a ratio of ≅ 8: 8: 1 for atoms S: Se: Cu which corresponds to the composition $(BETS)_2Cu(dca)_3$. The salt composition was confirmed by full X-ray diffraction analysis.

2.4. Synthesis of $(ET)_2Cu_{1.8}(dca)_4$ (**2**)

Crystals of **2** were obtained by electrochemical oxidation of ET (C1 = 0.010 g, 0.026 mmol) in the presence of a supporting electrolyte $(Ph_4P)Cu(dca)_3{\cdot}H_2O$ (*C*2 = 0.035 g, 0.057 mmol) + $Mn(dca)_2$-·(C3 = 0.012 g, 0.099 mmol) in a mixture of CB (9 mL)-benzonitrile (BN, 9 mL) – 96% ethanol (2 mL). Electrocrystallization was performed at constant current I = 0.4 μA at 25 C. The synthesis was carried out in a glass H-like two-electrode cell, similar to the cell used in synthesis of the crystals $BETS_2Cu(dca)_3$ (**1**). The electrodes were 1 mm-diameter platinum wire. The different shape crystals grew in the anode and cathode space for two to four weeks. The hexagon-like crystals as major phase formed with a small amount of long strip-shaped crystals on the anode, while the single octagonal-like crystals **2** unexpectedly formed only in the cathodic chamber volume of the electrochemical cell. Finally, the obtained crystals were filtered off, washed with acetone and dried in air. EPMA showed for **2** the presence of copper and sulfur atoms in a ratio of ≈2:8 and no Mn, in the hexagon-like crystals a S:Cu:Mn atom ratio of ≅ 8:1:1 and no metal in the composition of the strip-shaped crystals. Full X-ray analyses allowed to identify all of the obtained salts: the hexagon-like crystals were identified as **3**, the long strip-shaped crystals as the radical cation salt α''- $(ET)_2(dca){\cdot}2H_2O$ [27] and the octagonal-like crystals as $(ET)_2Cu_{1.8}(dca)_4$ (**2**).

2.5. Electron-probe X-ray microanalysis

EPMA of the radical cation salt crystals was performed with a Zeiss Supra-25 analytical field emission electron microscope equipped with a Gemini electron optical column at magnification varying from 600 to 6200 depending on the sample and the electron beam energy of 9.7–20 keV. The depth of beam penetration into the sample was 1–3 μm.

2.6. Transport measurements

Sample resistance was measured using a four-probe technique by a lock-in amplifier at 20 Hz alternating current. Two contacts were attached to each of two opposite sample surfaces with conducting graphite paste. In the experiment we have measured the out-of-plane resistance $R_\perp$ with the current running mainly perpendicular to conducting layers. The measurements in the temperature range (1.3 – 300) K were carried out in a cryostat with a variable temperature insert. The quasi-hydrostatic pressure was

applied to the sample using the Cu-Be clamp cell with silicon oil as a pressure medium and with the manganin probe for the pressure control.

2.7. Single crystal X-ray analysis

X-ray diffraction analysis was carried out on a CCD diffractometer Agilent XCalibur with EOS detector (Agilent Technologies UK Ltd, Yarnton, Oxfordshire, England). Data collection, determination and refinement of unit cell parameters was carried out using the CrysAlis PRO program suite [28]. X-ray diffraction data were collected for the crystals of **1** at 200 K and **2** at 100, 130 and 270 K using Mo Kα (λ = 0.71073 Å) radiation. The structure for both types of crystals was solved by direct methods followed by Fourier syntheses and refined by a full-matrix least-squares method in an anisotropic approximation for all non-hydrogen atoms by using the SHELX-97 program [29]. The positions of the hydrogen atoms were calculated geometrically.

The X-ray crystal structure data have been deposited with the Cambridge Crystallographic Data Centre, with reference code CCDC 1959558-1959561.

2.8. Electronic structure calculations

We use density functional theory to investigate the electronic structure of the three compounds **1**, **2** and **3**. We perform the calculations with the all electron full potential local orbital (FPLO) [30] basis set and generalized gradient approximation (GGA) [31] exchange correlation functional. We account for the strong correlations on the Cu and Mn 3d orbitals by a GGA + U [32] correction. In order to perform the electronic structure calculations, we have to deal with the partial occupations present in some of the structures. In $(BETS)_2Cu(dca)_3$, the central nitrogen of the dca group has two possible positions, both 50% occupied, allowing for the $P\,2_1/c$ space group. We choose one of the two nitrogen positions and thus lower the symmetry to *Pc*. In $(ET)_2Cu_{1.8}(dca)_4$ and $(ET)_2CuMn(dca)_4$, there are a few slightly disordered dca central nitrogen positions, and we perform the calculations choosing one of the two possibilities. There are also disordered ethylene end groups of the ET molecules, and we perform the calculations for the majority conformation.

2.9. Magnetic properties

We use an Elexys E500 spectrometer working in the X-band (9.4715 GHz) and modulated at 100 kHz. An RTI ESRCryo202 continuous flow cryostat refrigerated with liquid helium was used for cooling the samples down to 4.2 K.

3. Results and discussion

3.1. General procedure for synthesis of the crystals *1*–*3*

Complexes **1** and **2** were prepared by electrochemical oxidation of the matching π - donor: BETS or ET.

Electrochemical oxidation of the BETS donor was studied in various solvents: chlorobenzene (CB) + dichloromethane (DCM), benzonitrile (BN) + DCM, CB + 96% ethanol and 1,1,2-trichloroethane (1,1,2-TCE) + abs. ethanol. The solvents DCM, 96% ethanol and abs. ethanol were used as additives to basic solvents. The $(Ph_4P)Cu(dca)_3{\cdot}H_2O$ salt was used as electrolyte. In a mixture of CB with DCM (3–5 mL) hexagon- or rhombic like crystals **1** formed. The ratio of Cu: S: Se was determined by electron-probe X-ray microanalysis (ERMA) to be ~1: 8: 8, which corresponds to the composition $(BETS)_2Cu(dca)_3$. This preliminary composition of the salt was confirmed by its full X-ray analysis. When the amount of DCM was increased to 10 mL, another crystal phase including no copper atoms grew on the anode in the form of plates. Electrocrystalization of BETS in a mixture (CB + 96% ethanol) allowed for the synthesis of another phase in the form of elongated irregular hexagons, in which the ratio Cu: S: Se was equivalent to ~1: 4: 4. Such a ratio indicates the presence of Cu^{1+} and Cu^{2+} in the crystal with the most probable composition $(BETS)_2Cu_2(dca)_4$. Unfortunately, the insufficient quality of the crystals did not allow for analysis of their structure. Another possible composition of the salt with the same ratio of Cu: S: Se atoms corresponds to the formula of a simple salt with full charge transfer, $(BETS)Cu^{1+}(dca)_2$. However, the high salt conductivity (5–10 $Om^{-1}cm^{-1}$ at 300 K) and metal–insulator transition, observed at 70 K, indicates the presence in the structure of BETS radical cations with a charge of +0.5. Thus, the most likely composition is $(BETS)_2Cu_2(dca)_4$.

Electrocrystallization of BETS in two other solvent mixtures, (BN + DCM) and (1,1,2-TCE + abs. ethanol), was not accompanied by the growth of the crystals. The most suitable conditions for the preparation of salt **1** are given in the Experimental section.

Electrochemical oxidation of the ET donor was also studied in various solvents: CB, BN and their mixture, taken in the ratio 1:1, as well as in 1,1,2-TCE. In all experiments, 2% (by volume) of 96% ethanol (or abs. ethanol in 1,1,2-TCE) was added to the basic solvent. A mixture of $(Ph_4P)Cu(dca)_3{\cdot}H_2O$ and $Mn(dca)_2$ was used as electrolyte. Electrocrystallization of ET in both CB and its mixture with BN was accompanied by the growth of different crystals (**2**, **3** and metal-less salts), the quality and composition of which strongly depended on the initial conditions (nature of the basic solvent, temperature, concentration of the initial components, current and current density). In a mixture CB-BN solution the salt **3** was the main product of synthesis. It should also be noted that salt **3** was first obtained using the original technique in 1,1,2-TCE in the presence of an electrolyte consisting of a mixture of 18-crown-6 ether, Na(dca), CuBr (or CuCl) in a 1: 1: 1 M ratio and the simple salt $Mn(dca)_2$ [20]. In the case of using the mixture $(Ph_4P)Cu^{2+}(dca)_3{\cdot}H_2O$ + $Mn(dca)_2$ as an electrolyte, the presence of Cu^{1+} cations in salts **2** and **3** is probably associated with the reduction of divalent copper by ET and/or electrochemically at the cathode. Unlike salt **3**, salt **2** does not contain manganese according to ERMA analysis and includes copper in different degrees of oxidation. Refinement of crystal structure **2** showed that Cu^{2+} atom positions are not fully populated: $(ET)_2Cu^{1+}Cu^{2+}_{0.8}(dca)_4$. It should also be noted that, in contrast to the mixture of chlorobenzene with benzonitrile as a solvent, the use of an electrolyte $(Ph_4P)Cu(dca)_3{\cdot}H_2O$ + Mn(dca) in a medium of 1,1,2-trichloroethane led to the formation of plate crystals, an *ERMA* analysis of which showed the absence of copper in their composition.

3.2. Transport measurements

3.2.1. Conductivity of the salt *1*

Crystals of **1** and **2** were characterized by resistance measurements at ambient pressure, and pressures up to 10 kbar. At room temperature, the ambient pressure conductivity of crystals **1** is 8–10 $Ohm^{-1}cm^{-1}$ in the plane of the BETS layer. The temperature and pressure dependence of the resistance is shown in Fig. 1.

At ambient pressure, the sample resistance grows slowly with decreasing temperature, and then increases sharply below 30 K, indicating a phase transition to an insulating state. As seen from the Fig. 1, the application of pressure suppresses the metal–insulator transition; above P = 3 kbar, a metallic-like *R(T)* dependence is observed in the whole temperature region. In the insert *R(T)*, curves for the samples **1** and **4** at P = 0 in the vicinity of the metal–insulator transition are presented for comparison. One can see that for both samples the transition to the dielectric state takes place at about the same temperature, but for the sample **1** the

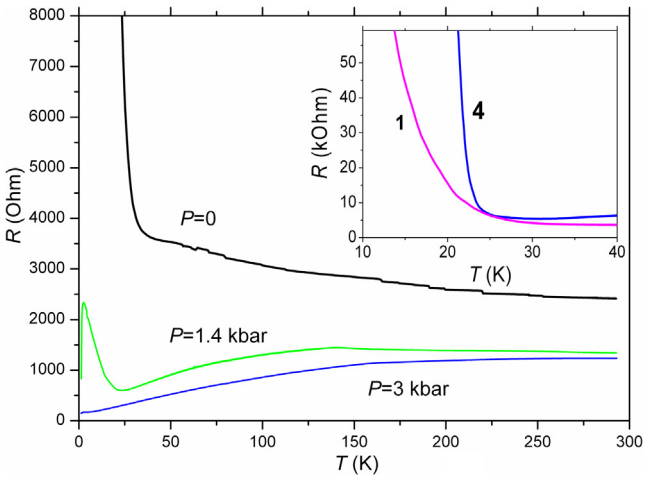

Fig. 1. The temperature dependences of the sample **1** resistance at different pressures. Indicated pressures refer to values measured at low temperature (15 K). In the insert *R(T)* curves for the samples **1** and **4** at *P* = 0 in the vicinity of the metal–insulator transition are presented.

transition is not so sharp. The salt **1** is isostructural with its Mn analog (**4**) (Section 3.3.1). Both salts have the same structure of the conducting κ-type BETS layers and their Fermi surfaces are similar [12,23] (Section 3.4.1). Therefore, we can assume that the metal–insulator transition in **1** has the same nature as the metal–insulator transition in **4.** A study of the transport and magnetic properties of salt **4**, as well as its ^{1}H and ^{13}C NMR spectra, showed that the transition of the BETS system into the insulating state is followed by localization of the π spins into a long-range ordered staggered structure of AF type [25,33,34]. However, it should be noted that, in contrast with the related Mn-based salt **4**, we did not find evidence for superconductivity at the studied pressures despite suppression of the metal–insulator transition.

3.2.2. Conductivity of the salt *2*

The room temperature conductivity of salt **2** is (1–3)·10^{-3}-Ohm^{-1}cm^{-1}. Fig. 2 demonstrates the temperature dependence of salt **2** resistance perpendicular to the conducting layers at different pressures. In this case, the pressure value *P* was determined at 300 K using the manganin probe. The *R(T)* curves show a remarkable hysteretic behavior in a very large temperature range (185 – 250 K), which unambiguously indicates the presence of a semiconductor I - semiconductor II phase transition. The hysteresis loop for **2** shifts to higher temperatures with pressure. As seen from the insert to Fig. 2, at *P* = 10 kbar the hysteresis loop is not observed. However, after removing the pressure, it is fully restored. As discussed in the next section, the phase transition is accompanied by changes in the charge state of the ET molecules as well as notable changes in the structure of the conducting and anion layer, especially in the environment of the Cu^{2+} ions.

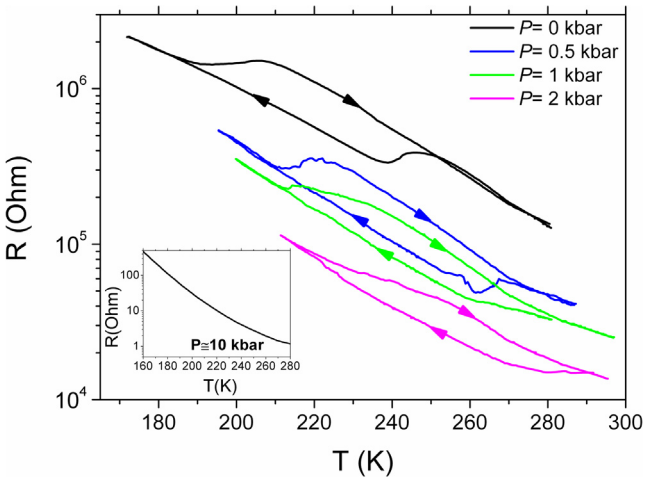

Fig. 2. Temperature dependences of the salt **2** resistance at different pressures. The inset shows the R(T) dependence without hysteresis at 10 kbar.

3.3. Structural analysis

The crystal structure of **1** was studied at a temperature of 200 K, while we investigated **2** at various temperatures from 100 to 270 K, in order to elucidate the nature of the first order transition in the range of 185 – 250 K (Transport measurements). Crystallographic parameters and the data collection and refinement statistics of salts **1** and **2** are given in Tables S1 and S2 (†ESI), respectively. Selected bond lengths and angles in structures **1** and **2** are listed in Tables S3-S5 (†ESI).

3.3.1. Structure of the crystals *1*

The BETS salt **1** is isostructural with its Mn (**4**) and the mixed Co-Mn (**5**) analogues. The crystal structure of the salt **1** is characterized by the alternation of κ-type organic radical cation layers with layers composed of polymeric {Cu[N(CN)$_2$]$_3$}$^-$ anions along the *a* axis of the unit cell (Fig. 3a). Fig. 3b demonstrates that the conducting layers of the crystals consist of dimers formed by BETS radical cations with a charge of ≈+0.5. In the dimer, radical cations are arranged in a "head to tail" type and have a "twist" conformation with the most effective way of overlapping BETS molecules in a dimer ("ring over bond" type). Such overlapping mode is realized in all superconductors with the k-type conducting layers [34,35]. The dihedral angle between adjacent dimers is 74.98°. A similar angle in the crystals **4** is less than about two degrees (72.80°) [11]. In contrast to the BETS$_2$Mn(dca)$_3$ salt, in which one of the terminal ethylene groups of BETS is disordered at room temperature, they are ordered in the copper salt **1**.

The polymeric {Cu[N(CN)$_2$]$_3$}$^-$ anion is formed by one crystallographically independent Cu^{2+} atom located in the inversion centre and three independent $N(CN)_2^-$ ligands located on general positions. Similar to the crystals **4**, each Cu atom has an octahedral environment and is bonded with six neighboring metal atoms via $\mu_{1,5}$-N(CN)$_2$ groups (Fig. 3c). The octahedron anion is notably distorted. In the direction of the coordination equatorial bonds N1—Cu1—N1 and N4—Cu1—N4 (2.198 and 2.286 Å bond length, respectively), it is elongated, while in the axial direction N3—Cu1—N3 (bond length 1.95 Å) it is flattened considerably. Selected angles of N—Cu1—N in the octahedron anion are given in Table S3 (†ESI). The observed distortions of the octahedron anion are probably related to the Jahn-Teller effect. In the salt **1**, one of the dicyanamide groups in the anion is statistically disordered.

In the structure of the radical cation layer there are several short intermolecular contacts: S···S (3.410–3.595 Å), Se···S (3.570 Å; 3.586 Å) as well as hydrogen bonds C—H···S (2.814 Å, 2.994 Å), and C—H···C (2.635 Å, 2.854 Å), Table 1. Additionally, to these contacts, each radical cation in the conducting layer is bound with the anion layer by one short S...N contact which is 3.253 Å and hydrogen bonds C—H···N (2.522 Å, 2.539 Å) and C—H···C (2.777 Å). The S...N contact is formed only with the central nitrogen atom of the —NC—*N*—CN-group, while the hydrogen bonds are formed by only the nitrogen of the CN$^-$ groups (Table 1).

3.3.2. Structure of the crystals *2*

Crystals of **2** are isostructural with those of **3**. Their structures are not typical of ET salts; most ET salts are specified by space sep-

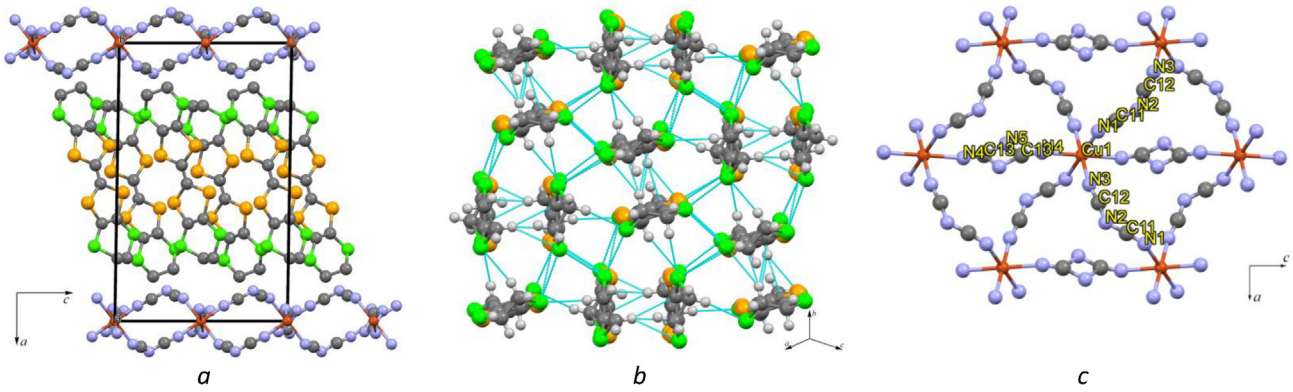

Fig. 3. (*a*) Crystal structure of **1** projected on the *ac*-plane. (*b*) The optimal view of the radical cation layer. Dashed lines show shortened contacts and H-bonds between BETS molecules. (*c*) Projection of the 2D polymeric anion of **1** on the *bc* plane with the designations of atoms in the anion.

Table 1
List of the short intermolecular contacts in the structure of the crystals **1.**

Short contact	Contact length, Å, at 200 K	Hydrogen bonds	Contact length, Å, at 200 K
Se1...S2[a]	3.586	H5B...S1[c]	2.814
S2...S4[a]	3.520	H5A...N4[d]	2.522
S1...S2[b]	3.410	H5A...N1[b]	2.539
S3...Se1[b]	3.570	H10A...C12[e]	2.777
S3...S4[b]	3.595	C3...H9B[f]	2.854
S1...N2[a]	3.253	C4...H9B[f]	2.635
		H5B...S1[c]	2.994

Symmetry operations for the second atom: [a] 1 − x, −y, 1 − z; [b] x, 1/2 − y, −1/2 + z; [c] 1 − x, −1/2 + y, 1/2 − z; [d] −x, 1/2 + y, 1/2 − z; [e] 1 − x, 1/2 + y, 1.5 − z; [f] 1 − x, 1 − y, 1 − z.

arated cationic and anionic subsystems. In **2**, the $Cu[N(CN)_2]_2$ structural fragments of the 3D $[Cu_{1.8}(dca)_4]^-$ anion network are built into 2D ET radical cation layers (Fig. 4a). An asymmetrical part of the unit cell of **2** includes four independent ET molecules (A, B, C, D) located in a special position in the center of symmetry and a magnetic 3D $[Cu_{1.8}(dca)_4]^-$ complex anion. The latter is formed by independent Cu^{1+} and Cu^{2+} atoms and four independent dicyanamide ligands. The complex anion consists of two interrelated structural fragments: 2D layers and the linear chains. The crystal structure of the salt, as well as the view of the radical cation layers and the anionic network are shown in Fig. 4.

The conducting layers of **2** formed by the ET radical cations have cavities occupied by the linear $\{Cu[N(CN)_2]_2\}^-$ fragments. The structure of the conducting ET layers is shown in Fig. 4b. The neighboring radical cations in the layers are linked with the short intermolecular S...S contacts. This type of cation radical layer packing was first discovered in **3** [20]. The atom numeration of the ET radical cations is presented in Fig. 5. Of four radical cations A, B, C and D, only in the cation D the terminal ethylene group is disordered. There are several short contacts S... S with a length of 3.431–3.580 Å and 3.460–3.594 Å, respectively at 130 and 270 K (Table 2). It should also be noted that the cooling of the crystal from 270 to 130 K leads to the increase of these contacts. Comparing the 130 K and 270 K structures, we find that the phase transition observed in the resistivity is occasioned by changes in the molecular geometry. However, the space group $P2_1/n$ remains at all temperatures, so the phase transition is not accompanied by a change of lattice symmetry.

On cooling the length of the central C=C bond decreases in C molecule (Δ = −0.015 Å), while the bond lengths in the other molecules A (Δ = +0.004 Å), B (Δ = +0,003 Å) and D (+0,005 Å) practically do not change in contrast to salt **3** [20]. Using the method of determining the charges of ET molecules [37], based on the analysis of the intramolecular bond lengths in ET, we estimated the charge states of molecules A, B, C, and D in structure **2**. The estimates showed that the charge states of molecules B and C are close to the neutral state (+0.2 to +0.4), while radical cations A and D have charges in the range of +0.85 to +1. Interestingly, in crystals **2**, the lengths of the valence bonds in the central part of the radical cations (TTF fragment) change less than in six-member rings (Table S4, †ESI), unlike other ET salts. This may be due to the considerable inclination of the molecules to each other (within 27°–87°) and the appearance of significantly shortened contacts between the radical cations and the anions, such as C...C, C...S, N...C and N...S (Table 2). At 130 K the radical cations have 3 (for A), 1 (for B and C) and 7 (for D) shortened contacts with the [N $(CN)_2$] ligands. In addition to the shortened contacts, hydrogen

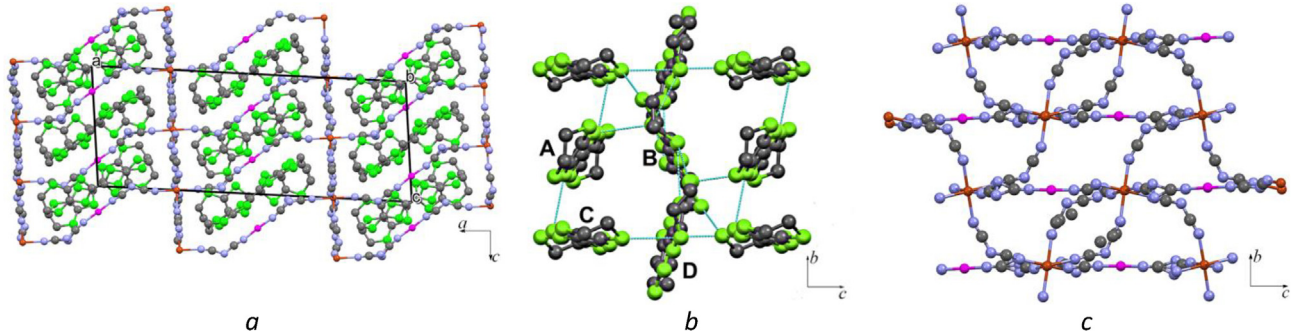

Fig. 4. (a) Crystal structure of **2** projected on the *ac*-plane. (b) The optimal view of the radical cation layer, dashed lines show shortened contacts between molecules ET. (c) Projection of the 2D polymeric anion of **2** on the *bc* plane.

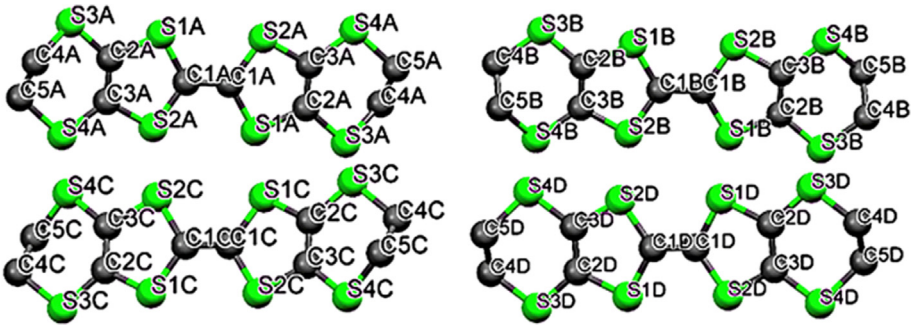

Fig. 5. The designations of ET radical cations A, B, C, D in the organic conducting layers of the salt **2**.

Table 2
List of short intermolecular contacts in the structure of the salt **2** at 130 K and 270 K.

Contact	Contact Length, Å		Contact	Contact Length, Å	
	130 K	270 K		130 K	270 K
S4C...S4D[a]	3.463	3.534	N2...C3B[a]	3.243	–
S1A...S1B[a]	3.536	3.594	N4′...C2D[a]	3.244	3.229
S2C...S2A[a]	3.459	3.523	N6...C4D[a]	3.228	–
S1A...S1B[a]	3.536	–	N4″...C5A[a]	3.229	–
S1B...S4D[a]	3.580	–	N4...S2C[a]	3.257	3.306
S4B...S3D[a]	3.431	3.460	N4′...S1D[a]	3.200	3.208
S4B...S1D[a]	3.551	3.591	N12...H4BB[a]	2.637	2.653
C1...S1A[a]	3.484	–	S3C...H4DA[b]	2.929	2.990
C1...S4D [a]	3.327	3.371	H5CA...S3B[a]	–	2.965
C2...S1D[a]	3.445	3.495	H5AA...S3D[c]	2.969	2.976
C6...S4D [a]	–	3.349	C8...H5BB[a]	–	2.728
C5...C5D[a]	3.395	–	C3...H5DB[a]	–	2.600
C5...C4D[a]	3.186	–	C7...H4BB[a]	2.713	2.768
N2...C2A[a]	3.162	3.234	C4...H5AB[a]	2.782	2.871

Symmetry operations for the first atom: [a] x, y, z; [b] 2 − x, 1 − y, 1 − z; [c] 1 − x, −y, 1 − z.

bonds S...H—C, N...H—C and C...H—C are also present in the salt structure. However, unlike the **3** salt, in the crystals **2** there are no intermolecular bonds between the 3*d* Cu^{2+} and S atoms. Lowering the temperature from 270 to 130 K also contributes to the rotation of the radical cations with respect to each other. Values of change in angles defined as the difference between the planes drawn through the central part of the radical cations are given in Table S5 (†ESI). The maximum rotation of the radical cations with respect to each other is equal to +2.17° for A-C and −2.36° for A-D molecules.

In the polymer anion the two-dimensional magnetic layers are formed by oblate Cu^{2+} coordination octahedra that are linked together by terminal nitrogen atoms of the ligands $[N(CN)_2]$. In the apical direction, octahedra are bound by terminal nitrogen atoms from linear fragments of $\{Cu^{1+}[N(CN)_2]_2\}^-$, Fig. 6.

The Cu^{2+}-N equatorial bonds (direction of N11, N9, N8, N5) are in the range 2.230–2.247 Å at 270 K and 2.229–2.245 Å at 130 K, while in the axial direction (N10, N7) they are 2.202–2.205 Å and 2.198–2.207 Å, respectively. Thus, the Jahn-Teller axes of the Cu^{2+} ions remain the same in the high and low temperature structures. In the equatorial plane the N-Cu^{2+}-N valence angles are in the range 88.25–90.37° at 130 K and 88.63–91.06° at 270 K. In the apical position, their values are 87.88–91.63° and 87.90–91.64° at 130 and 270 K, respectively,. In both cases, their magnitudes change little with cooling. The largest structural changes in the octahedral Cu^{2+} ions are observed in the Cu^{2+}-N—C angles. The equatorial angles differ from 180° markedly at each temperature and are in the range 160.1–178.9 (130 K) and, 157.3–177.3° at 270 K. The axial Cu^{2+}—N—C valence angles are 164.8° and 171.7° at 130 K, and 162.1° and 168.3° at 270 K. Their values increase by approximately 2% upon cooling through the first-order transition.

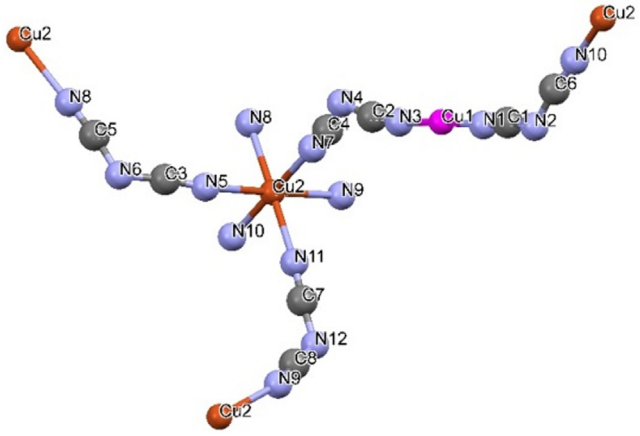

Fig. 6. The designations of atoms in the octahedron fragment of the $\{Cu_{1.8}[N(CN)_2]_4\}$ anion of the salt **2**.

For the linear dicyanamide chains penetrating the ET layers, the Cu^{1+}—N1 and Cu^{1+}—N3 bond lengths are equal to 1.828 Å and 1.827 Å at 270 K and 1.829 Å and 1.833 Å at 130 K (Fig. 6). In linear chains the magnitudes of the N—Cu^{1+}—N valence angles are 177.3° at 130 K and 178.1° at 270 K, respectively. When cooled, their values decrease by approximately 0.49%, which is noticeably less than in the case of the Cu^{2+}—N—C valence angles.

In the crystals **3,** unlike **2,** the Cu^{1+}—N bond lengths in the linear chains are 1.809 and 1.816 Å and 1.823 and 1.824 Å, respectively at 330 K and 291 K [20], *i.e.* noticeably less at the higher temperature. In radical cation salts of ET, including in their composition polymer

anion chains with a three-coordinate copper atom $\{Cu^{1+}[N(CN)_2]X\}^-$, where X = Cl and Br, the bond lengths of Cu^{1+}—N (1.941–2.053 Å) is longer than in $\{Cu[N(CN)_2]_2\}^-$ chains, which is the result of the presence of strongly electronegative Cl or Br atoms [35,36]. In the equatorial direction of the $[Cu^{1+}Cu^{2+}_{0.8}(dca)_4]$ anion, the valence angles C—N—C bonds, formed by the amide nitrogen atoms of two crystallographically independent ligands, $N(CN)_2^-$, are characterized by the values 121.5° and 121.6° at 130 K and 119.7° and 120.6° at 270 K. In the linking NCN—Cu^{1+}—NCN chain, similar angles at the same temperatures are equivalent to 125.3°, 126.3° and 124.5°, 124.4°. The latter practically do not change when the temperature is lowered from 270 to 130 K, in contrast to valence angles in chains connected with Cu^{2+} atoms, which increase by approximately 2°. In general, equatorial and apical coordinated ligands are considerably curved. Thus, the observed first-order phase transition is accompanied by noticeable structural changes in the radical cation layer as well as in a close environment of the Cu^{2+} ions.

3.4. Electronic structure calculations

3.4.1. Electronic structure of the crystals **1**

As noted in the Experimental Section, the symmetry of the structure was reduced to *Pc* for the purpose of the calculations, by fixing the positions of the disordered dca groups. Within the *Pc* unit cell, there are two formula units, which give rise to the bands near the Fermi level depicted in Fig. 7 at the generalized gradient approximation (GGA) level. The four BETS derived bands take the typical shape for the κ-type arrangement of the molecules [12,35,36,38]. Crossing these bands are four Cu 3*d* bands (from two Cu^{2+} ions), with $3d_{z2}$ and $3d_{x2-y2}$ character. In reality however, Cu^{2+} states are not expected at the Fermi level, and the more realistic electronic structure for crystal **1** is shown in Fig. 8. Here, we use a GGA + U functional with U = 8 eV on Cu 3*d* orbitals in order to account for the strong electronic correlation, and we mimic the expected paramagnetic state by an antiferromagnetic spin arrangement of Cu. As a consequence, Fig. 8 shows only BETS derived bands near the Fermi level. In order to determine the degree of charge transfer, we integrated the self-consistent charges [39]. We find 0.51 and 0.52 holes, respectively on the two symmetry inequivalent BETS molecules, indicating that the charge transfer is to very good approximation one hole per dimer. In order to check the possible influence of magnetism in the Cu anions on the BETS layers, we next considered spin-polarized solutions for the Cu ions using GGA + U with U = 8 eV as mentioned above. Without lowering the symmetry, only the ferromagnetic configuration is possible, which may not represent the minimum energy spin configuration. Nonetheless, we find the ferromagnetic configuration to be 176 meV lower in energy than the non-spin-polarized state, indicating that the Cu^{2+} ions will carry magnetic moments. Despite sizeable moments on the Cu atoms, DFT does not find spin polarization in the BETS molecules, and their band structure appears nearly unchanged. This may reflect relatively weak π-*d* interactions between the BETS and Cu subsystems.

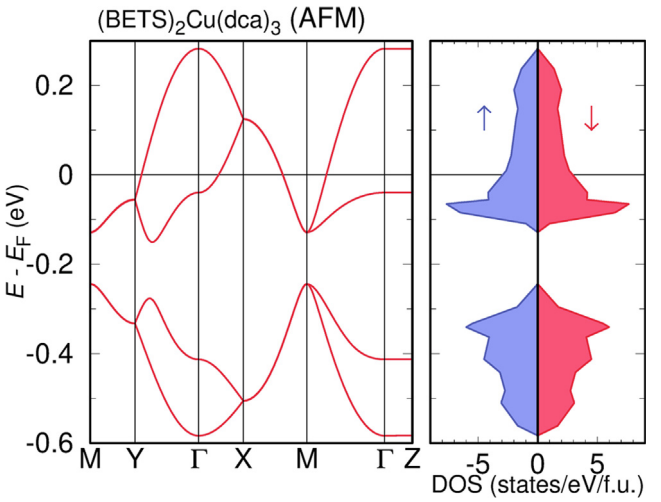

Fig. 8. Band structure and density of states (DOS) of **1** calculated using the all electron full potential local orbital (FPLO) basis at the GGA + U level with U = 8 eV on Cu 3*d* orbitals, choosing an antiferromagnetic configuration for Cu. The four bands close to the Fermi level E_F have pure BETS character.

In Fig. 8 we show the density of states (DOS) and bands near the Fermi level for an antiferromagnetic configuration of Cu spins. The corresponding BETS Fermi surface, shown in Fig. 9, consists of large ellipses that extend beyond the border of the Brillouin zone in k_z direction. This Fermi surface is similar to that of κ-$(BETS)_2Mn(dca)_3$ (**4**) (not shown) and κ-$(BETS)_2Co_{0.13}Mn_{0.87}(dca)_3$ (**5**) (see Ref. [21]). The Fermi surface resembles that of the κ-$(ET)_2X$ salts, [39,40,41] but the large ellipse has a more oblong shape in the present case.

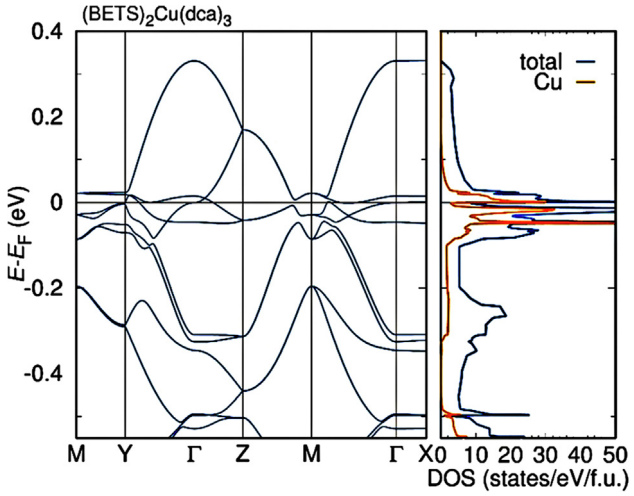

Fig. 7. Band structure and density of states (DOS) of **1** calculated using the all electron full potential local orbital (FPLO) basis at the GGA level.

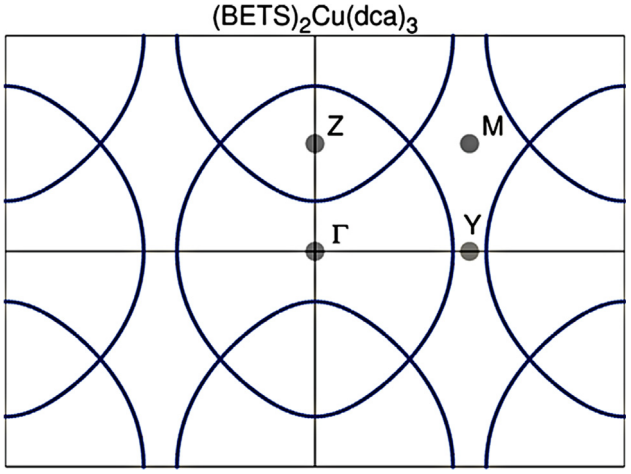

Fig. 9. Spin polarized Fermi surface of **1** calculated using FPLO in ferromagnetic configuration of the Cu moments. GGA + U with U = 8 eV is used to take into account strong correlations in Cu 3*d* orbitals.

*3.4.2. Electronic structures of the crystals **2** and **3***

In order to probe the nature of the first order transitions observed in **2** and **3**, we investigated using DFT the electronic structure and charge distributions of both salts as a function of temperature. Fig. 10 shows the computed band structure and density of states for the previously reported T = 291 K structure [20]. In order to account for the magnetic moments of the Mn^{2+} ions, we considered spin-polarized solutions at the GGA level, with Mn moments in a ferromagnetic configuration. The Mn^{2+} are found to be in a high-spin S = 5/2 state, with all 3d orbitals singly occupied, such that no Mn states appear near the Fermi level. Similarly, the majority of Cu states appear well below E_F, consistent with the formal +1 charge and $3d^{10}$ electronic configuration. The calculation cell contains four formula units. This leads to eight ET derived bands near the Fermi level. The bands display a quasi-1D form, with greatest dispersion along the Γ-Y path, corresponding to the monoclinic b-axis. This leads to nearly flat Fermi surface sheets running perpendicular to the k_y direction, as depicted in Fig. 11.

Fig. 12 shows the evolution of the charges on the ET molecules of **3** as function of temperature. This quantity is calculated by summing up the self-consistent GGA charges on all atoms of the ET molecules, with experimental structures taken as input for each temperature. These calculations reveal the nature of the sharp first order transition observed at 291 – 295 K in this material. For temperatures above T = 291 K, we find nearly equidistributed charges in the (A-C) chains while there is already a significant charge disproportionation of about 0.15 electrons in the (B-D) chains. Below T = 285 K, a strong charge order develops in the (A-C) chain, with a charge disproportionation of about 0.31 electrons. While the charge disproportionation in the B-D chains of 0.12 electrons is similar above and below the transitions, the charge rich B sites become charge poor below 291 K, while charge poor site D now becomes charge rich. Thus, we find the ET radical cations grouped into A-C chains and B-D chains. This can be understood as an electrostatic minimization of repulsion energy with the strong charges in the A-C chains. We thus find compelling evidence to view the first order transition as a rearrangement of the charge distribution in the ET layer, occasioned by a sharp charge order transition in the A-C chains. This finding is consistent with observed trends in the C=C bond lengths, [20] which are known to be sensitive to the local charges.

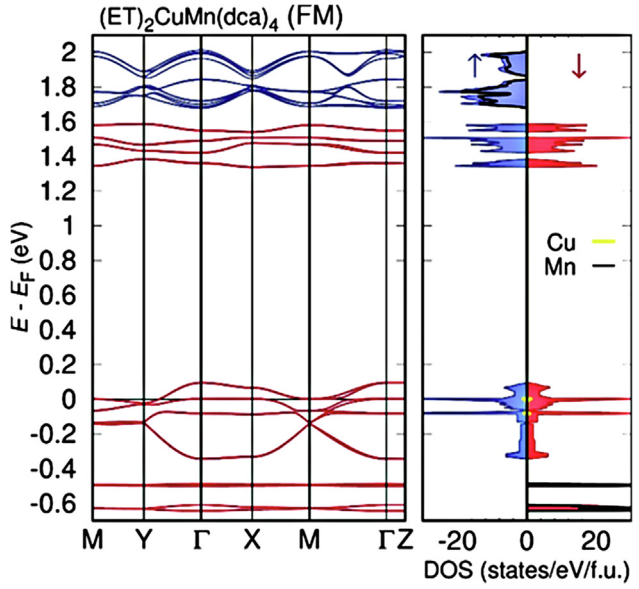

Fig. 10. Spin-polarized band structure and density of states (DOS) of **3** calculated using FPLO at the GGA level in the ferromagnetic configuration of the Mn moments. Red and blue indicate majority spin-up and spin-down bands, respectively. States near the Fermi energy E_F are composed primarily of ET states.

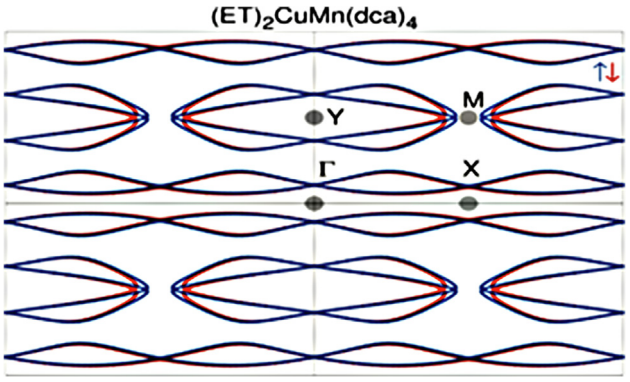

Fig. 11. Spin-polarized Fermi surface of **3** calculated using FPLO at the GGA level in the ferromagnetic configuration of the Mn moments. Red and blue indicate majority spin-up and spin-down bands, respectively.

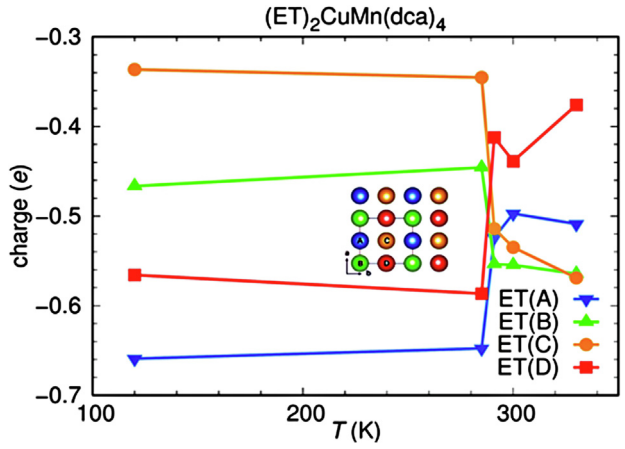

Fig. 12. The evolution of the charges on the ET molecules of **3** as function of temperature.

We now turn to the discussion of the Cu-based salt $(ET)_2Cu_{1.8}$(dca)$_4$ (**2**). In order to make calculations for compound **2** feasible, we neglect the Cu^{2+} deficiency and approximate $Cu_{1.8}$ as Cu_2. In Fig. 13, we show the band structure and DOS computed at the GGA level for the low-temperature 100 K structure. There are four Cu^{2+} ions that are octahedrally coordinated by nitrogen of dca, which exhibit partially filled bands of $3d_{x2-y2}$ character (see density of states plot). In contrast, the linearly coordinated Cu^{1+} ions have nearly no states near the Fermi level, consistent with the assignment of charges between the Cu atoms. When we allow for a magnetic solution the Cu^{2+} ions acquire a magnetic moment, while the Cu^{1+} remains nearly exactly nonmagnetic. The total moment for four formula units is 4.4 μ_B; however, rather than full S = 1/2 moment (as expected for Cu^{2+}), we find only 0.49 μ_B on each of the four Cu^{2+} ions. The rest of the moment is from spin-polarized ET molecules. In contrast with the mixed Cu/Mn salt (**3**), the octahedral Cu^{2+} ions contribute states at the Fermi level. This has a consequence for the Fermi surface shown in Fig. 14. Analysis of the orbital character shows that the spin up Fermi surface is entirely from Cu^{2+} while the spin down Fermi surface with one-dimensional sheets perpendicular to k_y arises from ET. This finding suggests strong antiferromagnetic π-d interactions in **2** between the ET and Cu^{2+} ions, which are not present in the mixed Cu/Mn salt **3**.

In Table 3, we show the charges on the constituents of $(ET)_2Cu_{1.8}$(dca)$_4$ calculated by summing up the self-consistent charges

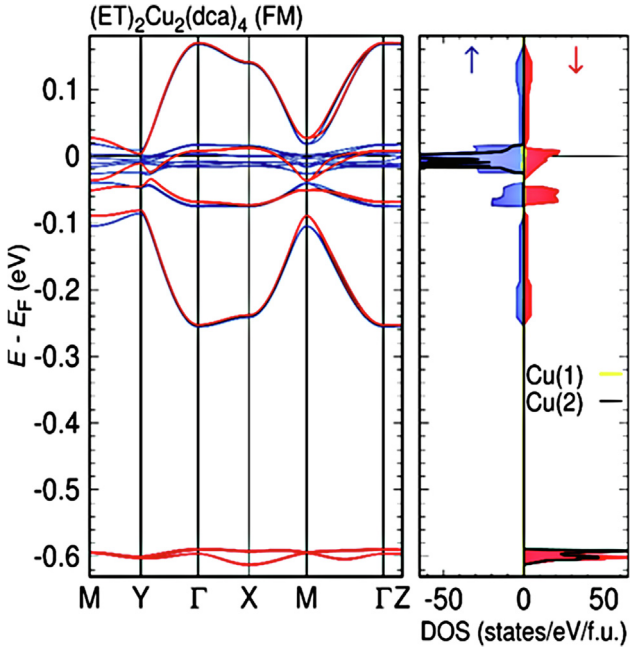

Fig. 13. Spin-polarized band structure and density of states (DOS) of **2** calculated using FPLO at the GGA level for the T = 100 K structure, and employing a ferromagnetic configuration.

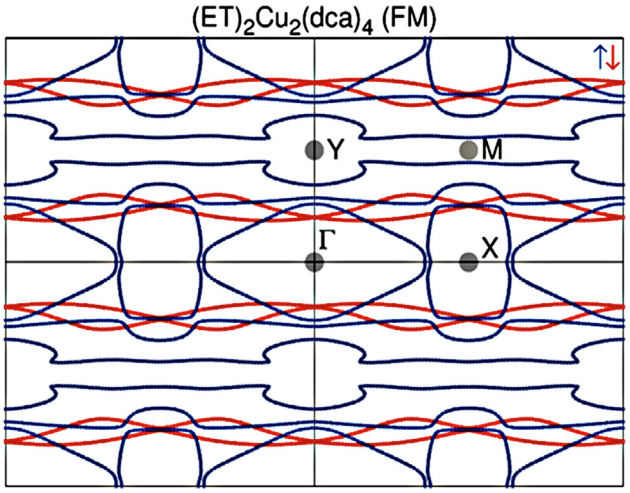

Fig. 14. Spin-polarized Fermi surface of **2** calculated using FPLO at the GGA level for the T = 100 K structure, and employing a ferromagnetic configuration of Cu moments.

on the atoms. The results clearly show the different valency of Cu^{1+} and Cu^{2+}, even though due to effects of covalency we cannot expect the charges on the metal ions to be integer numbers. Interestingly we find that the charge transfer is not complete. On average there are only 0.34 holes per ET molecule, rather than the ideal value of 0.5 holes. There is some charge disproportionation, in particular between charge rich ET1 and charge poor ET2 sites.

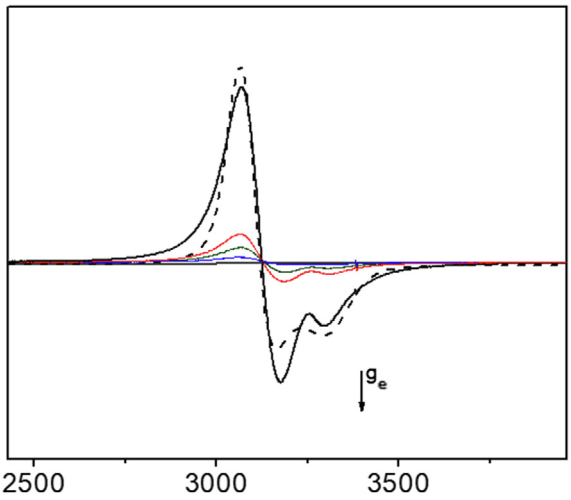

Fig. 15. The X-EPR spectra of powder samples of the salt **1** - (A) and **2** – (B). Solid gray lines – experiment at 5 K, dashed black lines – simulated spectra. The simulated powder spectrum of **1** for Cu^{2+} ion (S = ½) with g-factor $g_{\perp}$ = 2.1899 and $g_{||}$ = 2.0420. The simulated Lorenz derivative spectrum of **2** for ET donor S = 1/2 with g-factor g = 2.018 and linewidth lwpp = 150G. Microwave frequency 9.468586 GHz. Additionally, coloured lines show the temperature changes in the spectra at 17 K (red), 30 K (green) and 70 K (blue).

3.5. Magnetic properties

In order to observe the magnetic properties of **1** and **2**, the X-band EPR spectra was measured from 270 down to 5 K. Fig. 15 shows EPR spectra of polycrystalline samples of **1** and **2** at a temperature of 5 K, as well as temperature changes in the spectra up to 70 K.

The spectrum of compound **1** is a powder spectrum with axial anisotropy. It shows a weak dependence of the shape of the spectrum and its position over the entire temperature range. The shift of the g factor is common for Cu^{2+} ions (S = 1/2 with g-factor $g_{\perp}$ = 2.1899, $g_{||}$ = 2.0420). The hyperfine structure is not resolved. The spectrum amplitude monotonously increases with decreasing temperature. Since the quality of simulation of the anisotropic spectra of substance **1** is low and it is not possible to determine the signal from BETS, the only reliable parameter is the double integral of the entire spectrum. It is this (reciprocal) shown in Fig. 16 (trace A). This dependence has a point of inflection in the temperature range roughly corresponding to resistive measurements, in contrast to the monotonic dependence for substance **2** (trace B). The EPR spectrum of compound **2** at temperatures between 5 and 270 K is of Lorentzian line shape and shows a significant shift in the position of the line and its width with temperature (Fig. S1, see †ESI). These properties are usual for organic conductors based on the radical cation salts. The obtained EPR spectrum can be attributed to paramagnetic centers in the layer of the ET radical cations. ESR signals of Cu^{2+} with S = ½ for compound **2** were not detected.

For compound **1** the reciprocal integral EPR intensity follows the Curie-Weiss law from 5 to ~50 K with the estimated Weiss temperature T_{CW} = +1.6 K. The change in the temperature

Table 3
Self-consistent charges on the constituents of **2** at three different temperatures, calculated within GGA. Labels of the ET molecules correspond to the definitions in Fig. 4.

T (K)	$Cu[1](dca)_2$	$Cu[2](dca)_2$	ET1 (A)	ET2 (B)	ET3 (C)	ET4 (D)
100	−0.83	−0.54	0.40	0.36	0.29	0.32
130	−0.82	−0.54	0.41	0.33	0.27	0.35
270	−0.82	−0.55	0.41	0.33	0.29	0.35

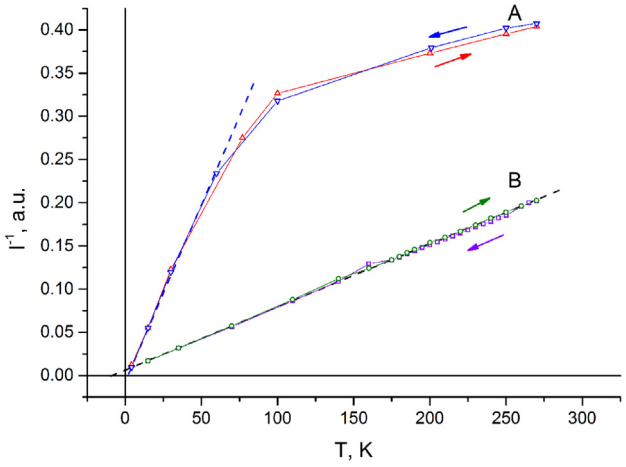

Fig. 16. Temperature dependencies during the cooling and heating cycle of reciprocal integral intensities EPR spectra of samples **1** - (A) and **2** – (B). Dashed lines show Curie-Weiss Law.

dependence behaviour of **1** in the 50 K region correlates with the MI phase transition defined by resistance measurements.

Compound **2** follows the Curie-Weiss law in the entire temperature range with Curie-Weiss temperature, T_{CW} = –8 K. No temperature hysteresis analogous to the resistivity measurement was found by EPR for the sample of **2**. In addition, no critical phenomena with temperature variation for magnetic parameters were detected (Fig. S1, †ESI).

4. Conclusion

The electrochemical oxidation of the organic donors ET and BETS in the presence of Cu dicyanamide counterions produces new salts $(BETS)_2Cu(dca)_3$ (**1**) and $(ET)_2Cu_{1.8}(dca)_4$ (**2**) with contrasting structural, electronic, and magnetic properties. The compounds represent Cu analogues of previously reported Mn salts, $(BETS)_2Mn(dca)_3$ (**4**) and $(ET)_2CuMn(dca)_4$ (**3**), offering a useful point of comparison. At ambient pressure, the resistance of compound **1** reveals a sharp metal–insulator transition at around 30 K. This transition is suppressed under mild pressures of 3 kbar, but we have not yet found evidence for a superconducting phase emerging, in contrast with the related Mn salt. The salt **2** undergoes a semiconductor I - semiconductor II phase transition in the range of 185 – 250 K, as evidenced by hysteretic jumps in the resistivity. Through a combination of structural analysis and first principles studies, we have identified this first order transition with a modification of the charge distribution between disparate ET molecules. Illuminating the microscopic driving force behind this transition represents an interesting future work. Taken together, these observations highlight the variety of phases that can be achieved in salts of organic donors with magnetic counterions.

CRediT authorship contribution statement

Nataliya D. Kushch: Conceptualization, Methodology, Writing - original draft. **Vyacheslav A. Kopotkov:** Visualization. **Gennady V. Shilov:** Formal analysis. **Alexander V. Akimov:** Investigation, Formal analysis. **Sergey V. Tokarev:** Investigation. **Eduard B. Yagubskii:** Supervision, Project administration, Writing - review & editing. **Vladimir N. Zverev:** Investigation. **Salavat S. Khasanov:** Investigation, Formal analysis. **Stephen M. Winter:** Investigation, Theory. **Harald O. Jeschke:** Investigation, Writing, Theory.

Declaration of competing interest

The authors declare that they have no known competing financial interests or personal relationships that could have appeared to influence the work reported in this paper.

Acknowledgments

We thank Prof. Akira Miyazaki for providing BETS used in the work and Dr. L. I. Buravov for test measurements of *R(T)* of some samples. The work was supported by the RFBR grants No. 17-03-00167 and 18-02-00280. The part of the work was done on the topic of the State task No. AAAA-A19-111902390079-8 with using of the Computational and Analytical Center for Collective Use of the IPCP RAS tool base.

Appendix A. Supplementary data

Supplementary data to this article can be found online at https://doi.org/10.1016/j.poly.2020.114705.

References

[1] L. Ouahab, Multifunctional Molecular Materials, Jenny Stanford Publishing, Singapore, 2013.
[2] T.G. Prokhorova, E.B. Yagubskii, Organic conductors and superconductors based on bis(ethylenedithio)tetrathiafulvalene radical cation salts with supramolecular tris(oxalato)metallate anions, Russ. Chem. Rev. 86 (2017) 164–180, https://doi.org/10.1070/RCR4655, and references therein.
[3] A.L. Morrit, J.R. Lopez, T.J. Blundell, E. Canadell, H. Akutsu, Y. Nakazava, S. Imajo, L. Martin, 2D molecular superconductor to insulator transition in the β"-(BEDT-TTF)$_2$[$(H_2O)(NH_4)_2M(C_2O_4)_3$]·18-crown-6 series (M = Rh, Cr, Ru, Ir), Inorg. Chem. 58 (2019) 10656–10664, https://doi.org/10.1021/acs.inorgchem.9b00292, and references therein.
[4] E. Ojima, H. Fujiwara, K. Kato, H. Kobayashi, H. Tanaka, A. Kobayashi, M. Tokumoto, P. Cassoux, Antiferromagnetic organic metal exhibiting superconducting transition, κ-(BETS)$_2$FeBr 4[BETS= Bis(ethylenedithio) tetraselenafulvalene], J. Am. Chem. Soc. 121 (1999) 5581–5582, https://doi.org/10.1021/ja990894r.
[5] H. Kobayashi, H. Cui, A. Kobayashi, Organic metals and superconductors based on BETS (BETS = Bis(ethylenedithio)tetraselenafulvalene), Chem. Rev. 104 (2004) 5265–5288, https://doi.org/10.1021/cr030657d.
[6] E. Coronado, J.R. Galan-Mascaros, C.J. Comez-Garsia, V. Laukhin, Coexistence of ferromagnetism and metallic conductivity in a molecule-based layered compound, Nature 408 (2000) 447–449, https://doi.org/10.1038/35044035.
[7] E. Coronado, P. Day, Magnetic molecular conductors, Chem. Rev. 104 (2004) 5419–5448, https://doi.org/10.1021/cr030641n.
[8] S. Uji, H. Shinagawa, T. Terashima, T. Yakabe, Y. Terai, M. Tokumoto, A. Kobayashi, H. Tanaka, H. Kobayashi, Magnetic-field-induced superconductivity in a two-dimensional organic conductor, Nature 410 (2001) 908–910, https://doi.org/10.1038/35073531.
[9] J. Balicas, S. Brooks, K. Storr, S. Uji, M. Tokumoto, H. Tanaka, H. Kobayashi, A. Kobayashi, V. Barzykin, L.P. Gorkov, Superconductivity in an organic insulator at very high magnetic fields, Phys. Rev. Lett. 87 (2001), https://doi.org/10.1103/PhysRevLett.87.067002, 067002 – 067002-4.
[10] E.S. Choi, D. Graf, J.S. Brooks, J. Yamada, A. Akutsu, K. Kikuchi, M. Tokumoto, Pressure-dependent ground states and fermiology in β–(BDA–TTP)$_2$MCl$_4$(M=Fe,Ga), Phys. Rev. B 70 (2004), https://doi.org/10.1103/PhysRevB.70.024517, 024517 – 024517-8.
[11] N.D. Kushch, E.B. Yagubskii, M.V. Kartsovnik, L.I. Buravov, A.D. Dubrovskii, A.N. Chekhlov, W. Biberacher, π-Donor BETS based bifunctional superconductor with polymeric dicyanamidomanganate(II) Anion Layer: κ-(BETS)$_2$Mn[N(CN)$_2$]$_3$, J. Am. Chem. Soc. 130 (2008) 7238–7240, https://doi.org/10.1021/ja801841q.
[12] V.N. Zverev, M.V. Kartsovnik, W. Biberacher, S.S. Khasanov, R.P. Shibaeva, L. Ouahab, L. Toupet, N.D. Kushch, E.B. Yagubskii, E. Canadell, Temperature-pressure phase diagram and electronic properties of the organic metal κ–(BETS)$_2$Mn[N(CN)$_2$]$_3$, Phys. Rev. B 82 (2010), https://doi.org/10.1103/PhysRevB.82.155123, 155123-155123-9.
[13] Y. Shen, G. Cosquer, B.K. Breedlove, M. Yamashita, Hybrid molecular compound exhibiting slow magnetic relaxation and electrical conductivity, Magnetochemistry 2 (2016), https://doi.org/10.3390/magnetochemistry2040044, 44–44-11.
[14] S. Ueki, T. Nogami, T. Ishida, M. Tamura, ET and TTF Salts with lanthanide complex ions showing frequency-dependent ac magnetic susceptibility, Mol. Cryst. Liq. Cryst. 455 (2006) 129–134, https://doi.org/10.1080/15421400600698287.
[15] N.D. Kushch, L.I. Buravov, P.P. Kushch, G.V. Shilov, H. Yamochi, M. Ishikawa, A. Otsuka, A.A. Shakin, O.V. Maximova, O.S. Volkova, A.N. Vasiliev, E.B. Yagubskii,

Multifunctional compound combining conductivity and single-molecule magnetism in the same temperature range, Inorg. Chem. 57 (2018) 2386–2389, https://doi.org/10.1021/acs.inorgchem.7b03152.
[16] G. Cosquer, Y. Shen, M. Almeida, M. Yamashita, Conducting single-molecule magnet materials, Dalton Trans. 47 (2018) 7616–7627, https://doi.org/10.1039/C8DT01015C, and references therein.
[17] S.R. Batten, K.S. Murray, Structure and magnetism of coordination polymers containing dicyanamide and tricyanomethanide, Coord. Chem. Rev. 246 (2003) 103–130, https://doi.org/10.1016/S0010-8545(03)00119-X.
[18] J. L. Manson in Magnetism: Molecules to Materials V, ed. J. S. Miller, M. Drillon, Wiley-VCH, Weinheim, 1ed, 2005, ch. 3, p.71.
[19] J. Schlueter, U. Geiser, J.L. Manson, Anionic dicyanamide frameworks as possible components of multifunctional materials, J. Phys. IV France 114 (2004) 475–479, https://doi.org/10.1051/jp4:2004114111.
[20] N.D. Kushch, A.V. Kazakova, A.D. Dubrovskii, G.V. Shilov, L.I. Buravov, R.B. Morgunov, E.V. Kurganova, Y. Tanimoto, E.B. Yagubskii, Molecular magnetic semiconductors formed by cationic and anionic networks: $(ET)_2Mn[N(CN)_2]_3$ and $(ET)_2CuMn[N(CN)_2]_4$, J. Mater. Chem. 17 (2007) 4407–4413, https://doi.org/10.1039/B706129C.
[21] N.D. Kushch, O.M. Vyaselev, V.N. Zverev, W. Biberacher, L.I. Buravov, E.B. Yagubskii, E. Herdtweck, E. Canadell, M.V. Kartsovnik, New radical cation salt κ-$(BETS)_2Co_{0.13}Mn_{0.87}[N(CN)_2]_3$ with two magnetic metals: Synthesis, structure, conductivity and magnetic peculiarities, Synth. Met. 227 (2017) 52–60, https://doi.org/10.1016/j.synthmet.2017.03.008.
[22] K.L. Nagy, B. Náfrádi, N.D. Kushch, E.B. Yagubskii, E. Herdtweck, T. Fehér, L.F. Kiss, L. Forró, A. Jánossy, Multifrequency ESR in $ET_2MnCu[N(CN)_2]_4$: a radical cation salt with quasi-two-dimensional magnetic layers in a three-dimensional polymeric structure, Phys. Rev. B 80 (2009), https://doi.org/10.1103/PhysRevB.80.104407, 104407 – 104407-8.
[23] O.M. Vyaselev, M.V. Kartsovnik, W. Biberacher, L.V. Zorina, N.D. Kushch, E.B. Yagubskii, Magnetic transformations in the organic conductor κ-$(BETS)_2Mn[N(CN)_2]_3$ at the metal-insulator transition, Phys. Rev. B 83 (2011), https://doi.org/10.1103/PhysRevB.83.094425, 094425 – 094425-6.
[24] O.M. Vyaselev, N.D. Kushch, E.B. Yagubskii, Proton NMR study of the organic metal κ- $(BETS)_2Mn[N(CN)_2]_3$, JETP 113 (2011) 835–841, https://doi.org/10.1134/S106377611114010X.
[25] O.M. Vyaselev, R. Kato, H.M. Yamamoto, M. Kobayashi, L.V. Zorina, S.V. Simonov, N.D. Kushch, E.B. Yagubskii, Properties of Mn^{2+} and π-electron spin systems probed by ^1H and ^{13}C NMR in the organic conductor κ-$(BETS)_2Mn[N(CN)_2]_3$, Crystals 2 (2012) 224–235, https://doi.org/10.3390/cryst2020224.
[26] J.A. Schlueter, J.L. Manson, K.A. Hyzer, U. Geyser, Novel anionic dicyanamidocuprate(II) structural motifs through cation templation, Polyhedron 26 (2007) 2264–2272, https://doi.org/10.1016/j.poly.2006.11.021.
[27] A.V. Kazakova, N.D. Kushch, A.N. Chekhlov, A.D. Dubrovskii, E.B. Yagubskii, K.V. Van, New multicomponent organic semiconductors based on ET with polymeric Anions: α''-$(ET)_2N(CN)_2{\cdot}2H_2O$ and α'''-$(ET)_6(NO_3)_3{\cdot}2C_2H_5O_2N_3$, Russ. J. Gen. Chem. 78 (2008) 6–13, https://doi.org/10.1134/S1070363208010027.
[28] CrysAlis PRO, Version 171.35.19, Oxford Diffraction Ltd., Oxford, UK, 2011.
[29] Sheldrick G.M. (8/06/2000). SHELXTL v. 6.14, Structure Determination Software Suite, Bruker AXS, Madison, Wisconsin, USA, 2000.
[30] K. Koepernik, H. Eschrig, Full-potential nonorthogonal local-orbital minimum-basis band-structure scheme, Phys. Rev. B 59 (1999) 1743–1759, https://doi.org/10.1103/PhysRevB.59.1743.
[31] J.P. Perdew, K. Burke, M. Ernzerhof, Generalized gradient approximation made simple, Phys. Rev. Lett. 77 (1996) 3865–3868, https://doi.org/10.1103/PhysRevLett.77.3865.
[32] A.I. Liechtenstein, V.I. Anisimov, J. Zaanen, Density-functional theory and strong interactions: orbital ordering in Mott-Hubbard insulators, Phys. Rev. B 52 (1995) R5467–R5470, https://doi.org/10.1103/PhysRevB.52.R5467.
[33] O.M. Vyaselev, M.V. Kartsovnik, N.D. Kushch, E.B. Yagubskii, Staggered spin order of localized π-electrons in the insulating state of the organic conductor κ-$(BETS)_2Mn[N(CN)_2]_3$, JETP Lett. 95 (2012) 565–569, https://doi.org/10.1134/S0021364012110100.
[34] O.M. Vyaselev, W. Biberacher, N.D. Kushch, M.V. Kartsovnik, Interplay between the *d*- and π-electron systems in magnetic torque of the layered organic conductor κ-$(BETS)_2Mn[N(CN)_2]_3$, Phys. Rev. B 96 (2017), https://doi.org/10.1103/PhysRevB.96.205154.
[35] J.M. Williams, R.J. Ferraro, R.J. Thorn, K.D. Carlson, U. Geiser, H.H. Wang, A.M. Kini, M.-H. Whangbo, in: Organic Superconductors (Including Fullerenes), Prentice Hall, Englewood Cliffs, NJ, 1992, https://doi.org/10.1002/ange.19941061238.
[36] N.D. Kushch, A.V. Kazakova, L.I. Buravov, A.N. Chekhlov, A.D. Dubrovskii, E.B. Yagubskii, E. Canadell, The first polymorph, κ''-$(ET)_2Cu[N(CN)_2]Cl$, in the family of κ-$(ET)_2Cu[N(CN)_2]X$ (*X*=Cl, Br, I) radical cation salts, J. Solid State Chem. 182 (2009) 617–621, https://doi.org/10.1016/j.jssc.2008.10.035.
[37] P. Guionneau, C.J. Kepert, G. Bravic, D. Chasseau, M.R. Truter, M. Kurmoo, P. Day, Determining the charge distribution in BEDT-TTF salts, Synth. Met. 86 (1997) 1973–1974, https://doi.org/10.1016/S0379-6779(97)80983-6.
[38] C.H. Kandpal, I. Opahle, Y.-Z. Zhang, H.O. Jeschke, R. Valentí, Revision of model parameters for κ-type charge transfer salts: an Ab initio study, Phys. Rev. Lett. 103 (2009), https://doi.org/10.1103/PhysRevLett.103.067004, 067004 – 067004-4.
[39] M. Souto, H.-B. Cui, M. Peña-Alvarez, V.G. Baonza, H.O. Jeschke, M. Tomic, R. Valentí, D. Blasi, I. Ratera, C. Rovira, J. Veciana, Pressure-induced conductivity in a neutral nonplanar spin-localized radical, J. Am. Chem. Soc. 138 (2016) 11517–11525, https://doi.org/10.1021/jacs.6b02888.
[40] D. Guterding, S. Diehl, M. Altmeyer, T. Methfessel, U. Tutsch, H. Schubert, M. Lang, J. Müller, M. Huth, H.O. Jeschke, R. Valentí, M. Jourdan, H.-J. Elmers, Evidence for eight-node mixed-symmetry superconductivity in a correlated organic metal, Phys. Rev. Lett. 116 (2016) 237001–237001–7, https://doi.org/10.1103/PhysRevLett.116.237001.
[41] D. Guterding, M. Altmeyer, H.O. Jeschke, R. Valentí, Near-degeneracy of extended $s+d_{x2-y2}$ and d_{xy} order parameters in quasi-two-dimensional organic superconductors, Phys. Rev. B 94 (2016), https://doi.org/10.1103/PhysRevB.94.024515, 024515 – 024515-13.